M. Olsson, P. van Belle, S. Conroy, T. Elevant, G. Sadler
and JET Team

Analysis of Neutron Energy Spectra from Neutral Beam Heated Plasmas in the JET Tokamak

Analysis of Neutron Energy Spectra from Neutral Beam Heated Plasmas in the JET Tokamak

M. Olsson[1], P. van Belle, S. Conroy, T. Elevant[1], G. Sadler
and JET Team*

JET-Joint Undertaking, Culham Science Centre, OX14 3DB, Abingdon, UK

[1]*Alfven Laboratory, KTH, Stockholm, Sweden*
* See Annex

ABSTRACT.

Neutron energy spectra from deuterium neutral beam heated plasmas at the Joint European Torus (JET) have been measured with a time-of-flight spectrometer. The different source fractions, resulting from thermal-thermal (tt), beam-thermal (bt) and beam-beam (bb) interactions have been extracted. The measured tt fraction and associated ion temperature is checked for consistency with diagnostic data for electron density n_e, effective charge Z_{eff}, ion temperature T_i and total neutron emission. Two different ways of comparing the data are presented. Firstly, the measured tt fraction, total neutron emission, n_e, Z_{eff} and T_i profile shape are used to deduce a consistent T_i, which is compared with T_i values obtained independently by other diagnostics. Secondly, the measured tt fraction, total neutron emission, ne profile shape and T_i are used to determine a consistent thermal deuterium density no, which is compared with no obtained from Z_{eff} measurements. The experimental errors from the analysis of the neutron spectra can be reduced by carefully restricting the analysis to plasmas within well defined ranges of ion temperature and tt fraction. The values of T_i and no thus derived are in good agreement with the values obtained independently. The method demonstrated in this paper can therefore be used with confidence to obtain plasma parameters under conditions which lie outside the operating range of the more conventional diagnostics, provided these conditions are met.

Contents

1 Introduction

During recent years, large fusion experiments based on the tokamak concept like the Joint European Torus (JET) in Europe and the Tokamak Fusion Test Reactor (TFTR) in the USA, have routinely produced substantial numbers of D-D neutrons. Considerable efforts have been made to use the emitted neutrons for diagnostic purposes [1-3]. The most desired quantities are the total neutron emission, the spatial neutron source distribution and the neutron energy distribution. At JET, a comprehensive set of neutron diagnostics is routinely used [4]. It consists essentially of a time resolved neutron yield monitor, a 19-channel profile camera and neutron spectrometers. The neutron yield is a direct measure of the fusion reaction rate in the plasma and thus a measure of the fusion power. Neutron emission profiles can be used to deduce transport properties of the plasma and to study MHD activity such as sawtooth oscillations [5]. Neutron spectrometers are used to investigate the origin of the emitted neutrons and to deduce information on the velocity distribution of the reacting ions.

Neutrons are generated by various mechanisms in a tokamak operating with deuterium. Thermonuclear D-D reactions involving deuterons with a Maxwellian velocity distribution give thermal-thermal (tt) neutrons with an essentially Gaussian energy spectrum; where the peak width is a measure of the ion temperature [6]. In the case of auxiliary heating by means of deuterium neutral beam injection (NBI) or ion cyclotron resonance frequency (ICRF) heating, a non-Maxwellian deuteron velocity distribution can build up, giving rise to NBI or ICRF induced D-D neutrons. For example, deuterons in the non-Maxwellian distribution resulting from deuterium NBI, reacting with deuterons from the same distribution, produce beam-beam (bb) neutrons. They also react with thermal deuterons from the Maxwellian distribution of the target plasma and give beam-thermal (bt) neutrons. The tt, bt and bb neutrons have, in principle, different energy spectra [6]. During high power (>5MW) ICRF heating of plasmas with beryllium as the main impurity, reactions between ICRF-accelerated ions in the MeV range and beryllium impurity ions may also produce a substantial number of neutrons [7]. The energy spectrum of these neutrons is however different from that of D-D neutrons. Finally, in connection with plasma disruptions, very short, high intensity bursts of photo neutrons are observed [8].

The time resolved neutron yield monitor measures the total neutron emission rate and does not discriminate between neutrons produced by the different mechanisms. Therefore, the additional information from the neutron spectrometers is essential for the

interpretation. However, even though the various neutron-producing mechanisms give rise to neutron energy spectra with different shapes, these spectra overlap to a large extent, rendering the interpretation difficult. In the case of deuterium neutral beam heated hot-ion plasmas ($T_i > 15 keV$) the distinction of the tt, bt and bb components for an injection energy $E_b = 80$ keV seems almost impossible. This is discussed in greater detail in sec 3.1. In the following sections of this report we analyse neutron energy spectra measured during deuterium NBI heating, check the results for consistency with other diagnostic data and assess to what extent useful information can be deduced. In particular, the method demonstrated in this paper has potential applications for obtaining the deuterium density, n_D, under conditions which lie outside the operating range of the more conventional diagnostics. It is therefore of interest to investigate the reliability of the method by comparison with results from other diagnostics under plasma conditions where these provide reliable data.

2 Method

2.1 Spectrum analysis

The neutron spectra discussed here are measured with a time-of-flight spectrometer [9], which is located in the JET roof laboratory, fig 1. The instrument has a vertical line-of-sight through the plasma and provides about one useful spectrum (>500 counts) per second during auxiliary heating, resulting in 1 to 5 spectra per JET discharge. Typical spectra are shown in fig 2. Fig 2a shows a spectrum from an ICRF heated discharge; the shape appears to be Gaussian and there is no sign of neutrons due to fast (non-Maxwellian) ions. Moreover, the ion temperature deduced from the width of the spectrum is in agreement with other diagnostics. Fig 2b is from a discharge with deuterium NBI only ($E_b = 80$ keV); the spectrum is considerably broader due to the higher mean energy of the reacting ions. In fig 2c, the effects of intense ICRF heating combined with NBI, in a plasma with beryllium as the main impurity, are shown. The spectrum is very broad with pronounced wings due to reactions between ICRF-accelerated ions and the beryllium impurity ions and/or reactions between ICRF-accelerated deuterons and thermal deuterons.

The method used to analyse the spectra is similar to that applied in [10]. The neutron spectrum is assumed to be built up of components corresponding to the various neutron-producing mechanisms, i.e. thermal-thermal (tt), beam-thermal (bt) and beam-beam (bb) interactions. The spectral shapes of these components can be calculated from the velocity distributions of the interacting ions. The FPS-code [6]

utilizes a Monte-Carlo method to numerically calculate these shapes; ion velocities are sampled at random from theoretical velocity distributions and the corresponding reactivity contributions and neutron energies are calculated and added up for a large number of samples ($> 10^6$) to form the desired neutron spectrum for a given line of sight. Pre-calculated spectra from the FPS-code for the different components are folded with the instrumental response and fitted to the measured spectrum using a maximum likelihood method [11]. The amplitudes of the different components are left as free parameters, to be determined by the fitting procedure. In figs 3a - 3d, the analysis of the spectrum from fig 2b is illustrated. Fig 3a shows the FPS-calculations of the bb and bt components for a target deuterium plasma with $T_e=T_i=5keV$, together with the corresponding Gaussian for the tt component. These are folded seperately with the instrumental response; the results are shown in fig 3b. In fig 3c, the resulting fit of the folded bb, bt and tt spectra to the measured spectrum can be seen. The deduced fractional bb, bt and tt contributions are: 0.08, 0.62 and 0.30, respectively. Finally, the underlying neutron spectrum is obtained by adding up the non-folded bb, bt and tt spectra accordingly, as shown in fig 3d.

The width and mean energy of the Gaussian neutron spectrum from tt reactions are known functions of the ion temperature T_i [6]. Therefore, T_i could, in principle, be left as a free parameter for the fitting routine to determine. In practice, this is of limited value for discharges where many pre-calculated spectral shapes have to be used in the analysis, as the uncertainty on T_i values determined this way is large unless the tt fraction is dominant (>50%). A measured neutron spectrum consists of a finite number of energy channels and, hence, contains a limited amount of information. For each extra parameter that is deduced by the fitting procedure, the uncertainties on all the fitted parameters increase. For this reason, neutron spectra from discharges with many neutron producing mechanisms are difficult to analyse. Therefore, for discharges where the tt neutron emission is not dominant, T_i is obtained with much better accuracy from other JET diagnostics such as active charge exchange recombination spectroscopy (CXRS) [12], or measurement of the doppler broadening of an impurity X-ray line (XCS) [13]. Taking T_i from one of these sources also helps to keep the number of free parameters to a minimum in the described data fitting.

Another restriction is that the velocity distributions for the reacting ions must be known, in order to pre-calculate spectra with the FPS-code. For a non-Maxwellian ion velocity distribution, this is obtained as the solution to the Fokker-Planck equation. Reasonably accurate solutions exist for NBI [14], while at present, existing solutions for ICRF-driven ions are not useful as they are very sensitive to the density of the

minority ions (protons), to which the ICRF is tuned; unfortunately, this density is a poorly known quantity. Therefore, no detailed quantitative analysis has been performed so far on neutron spectra showing signs of ICRF-induced neutrons, although in [7] the contribution to the neutron emission from ICRF-driven ions has been estimated in some cases.

For the reasons mentioned above, only NBI-heated discharges are treated in the following sections. The injectors provide deuterium neutrals at one half and one third of the nominal energy as well as at the nominal energy. The reactivity of these lower energy components is negligible for 80 keV NBI but becomes important for 140 keV NBI. The number of quantities to be determined by the fitting of the neutron spectra is kept low by selecting discharges with 80 keV NBI only, deliberately avoiding discharges with a mixture of 80 keV and 140 keV NBI. The inclusion of 140 keV NBI would make it necessary to use more pre-calculated spectra, thereby increasing the number of fitting parameters and consequently the associated error bars. In the work presented in this paper only three pre-calculated spectral shapes (tt, bt and bb) are used and the spectrum analysis program determines their relative intensities.

2.2 Consistency check

The tt contribution to the global neutron yield is a function of the thermal deuteron density profile, $n_D(r)$, and the ion temperature profile, $T_i(r)$, where r is the minor radial position in the plasma, i.e. r = 0 is the plasma center. The local Z_{eff} is defined as

$$Z_{eff} = \sum_i \frac{n_i \cdot Z_i^2}{n_e} \qquad (1)$$

where the sum is over all ion species "i" in the plasma, n_i is the ion density, Z_i is the ion charge number and n_e is the electron density. Assuming a flat effective charge profile $Z_{eff}(r)$, $n_D(r)$ can be deduced from the electron density profile, $n_e(r)$, and Z_{eff}, provided the impurity mixture is known. In some cases $n_D(r)$ profiles are available directly from CXRS measurements and these show that a flat $Z_{eff}(r)$ profile is usually a reasonable assumption for the purposes of the present analysis. Averaged values of the available data have been used in this paper.

The electron density profile, $n_e(r)$, is deduced from interferometric measurements [15], and Z_{eff} is obtained from visible bremsstrahlung measurements [16]. $n_e(r)$ is also measured by the LIDAR Thomson scattering diagnostic [17], at 1 s

intervals, which is too infrequent to be directly used in our analysis. Usually, the LIDAR $n_e(r)$ profiles show detailed features that are not present in the profiles obtained by inversion of the line-integrated data from the interferometer channels; resulting discrepancies (up to 30% in extreme cases) have to be taken into account when evaluating the uncertainties of the final results. These discrepancies are due to the limited number ($\leq$ 6) of available interferometer channels leading to a parametrization of $n_e(r)$ in the inversion procedure, which cannot reproduce fine details in contrast to LIDAR, which yields a direct measurement of the local n_e with good spatial resolution. For the analysis described in the present paper, $n_e(r)$ values averaged over periods of typically 1s have been used and only minor discrepencies were encountered.

$T_i(r)$ is usually obtained from CXRS. When CXRS data are not available, $T_i(0)$ is taken from XCS and the profile shape is assumed to be the same as for the electron temperature $T_e(r)$, measured by the electron cyclotron emission (ECE) diagnostic [18]. This is usually a good assumption, except for hot-ion mode plasmas which, also for other reasons, are not analysed in this paper (see sec. 1.).

The interpretation of the data relies on the use of the "ORION" code [19]. In this code n_D, T_i, n_e, Z_{eff}, the neutron emissivity S_n and other local quantities are assumed to be functions of the magnetic flux surface index Ψ and time only.

ORION calculates the thermal neutron emission profile, $S_{tt}(\Psi) = \frac{1}{2}n_D(\Psi)^2 <\sigma v>(\Psi)$, from the measured $n_D(r)$ and $T_i(r)$ profiles and performs an integration of this profile along the line-of-sight of the time-of-flight spectrometer.

By using a χ^2–minimization technique, ORION also computes the total (as opposed to thermal) neutron emissivity $S_n(\Psi)$ from the line-of-sight integrated neutron emissivities as measured by the neutron profile camera. The line integrals of the profile camera are computed for an assumed analytical emission profile $S_n = f(\Psi,a,b,c,d,...)$, where a,b,c,d.. are parameters characterizing the shape of the profile. The results are compared with measured data, and the discrepancy is minimized by variation of the parameters, until the best possible fit is obtained. Finally, the total emissivity is integrated along the spectrometer's line-of-sight.

The ratio of the two line integrals yields a calculated tt fraction, $f_{tt,calc}$, of the collimated neutron flux, which should be the same as the tt fraction obtained from the neutron spectrum analysis, $f_{tt,Spectrum}$; i.e.

$$f_{tt,calc} = f_{tt,Spectrum}$$ (2)

$$f_{tt,calc} = \frac{V_{tt,calc}(n_D, T_i)}{V_{tot,calc}}$$ (3)

$$f_{tt,Spectrum} = \frac{V_{tt,Spectrum}(T_i)}{V_{tot,Spectrum}}$$ (4)

where V_{tt} and V_{tot} are the line of sight integrated thermal and total emissivities respectively.

The calculated tt fraction depends on both the central values and the profile shapes of n_D and T_i. However, the shape dependence is much weaker than the dependence on the central values and have negligible influence on the results presented below. Equation (2) to (4) can be exploited in two different ways: a) n_D values from the optical diagnostics are used and T_i is iterated until agreement is achieved leading to consistent values of T_i, b) T_i values from other diagnostics are used and consistent values of n_D are deduced. Both approaches are treated in the next section.

3 Analysis

3.1 Consistent T_i deduction

The measured neutron spectrum is analysed repeatedly using a range of Ti values for the Gaussian tt component and the pre-calculated bt and bb shapes. The tt fraction, $f_{tt,spectrum}$, is mapped out as a function of these assumed values. The tt fraction, $f_{tt,calc}$, is also calculated for a similar range of central T_i values using the ORION code with the measured $n_D(r)$ profile. The measured $T_e(r)$ profile shape scaled to the assumed central T_i value is used in the calculation. The resulting two curves are shown in fig 4. Agreement between the neutron spectrum analysis and the calculated tt fraction is obtained for the value of T_i at which the curves intersect. This is the central T_i value for which the measured neutron energy spectrum, $n_D(r)$ and the T_e profile shape are consistent. This value is only weakly dependent on the $T_e(r)$ and $n_D(r)$ profile shapes as was pointed out above, and thus is mainly determined by the tt fraction from the neutron spectrum analysis and the central n_D as measured by the

9

optical diagnostics. In summary: measured neutron spectra, central n_D values and profile shapes are used to deduce consistent central T_i values.

Fig 5 shows the database of consistent central T_i values as a function of central T_i values measured by CXRS or XCS. The scatter of the data points is reduced if data points for which the tt fraction < 0.3 or T_i > 12 keV or $n_D(0)/n_e(0)$ < 0.4 are omitted, as seen from the encircled data points. The first restriction is justified by the difficulty to extract with confidence a small tt fraction because of the statistical fluctuations of the dominating (bt and bb) components in the neutron spectrum; i.e. the Poisson noise in the measured spectrum obscures the tt component, unless this component is sufficiently large. The reason for the second restriction is that the spectral shapes of the tt, bt and bb components become very similar when T_i approaches 20 keV (for 80 keV NBI) and thus the analysis becomes less reliable. If one were to study discharges with 140 keV NBI, this critical temperature would be higher. The last restriction is because the accuracy in n_D obtained from the CXRS or the visible bremsstrahlung measurement is best when $n_D(0)/n_e(0)$ is close to unity and deteriorates with decreasing values.

3.2 Consistent n_D deduction

Here the value of n_D, which is consistent with the tt fraction obtained from the neutron spectrum analysis and the T_i value obtained from CXRS or XCS, is deduced. Firstly, the tt fraction, $f_{tt,Spectrum}$ (eq(4)), is obtained from neutron spectrum analysis, taking the T_i value from CXRS or XCS diagnostics. Secondly, ORION is used to calculate the tt fraction along the line-of-sight of the neutron spectrometer, $f_{tt,calc}$ (eq(3)), from the measured $T_i(r)$ profile and a deuterium density profile, $n_D(r)$, which is set equal to the measured $n_e(r)$ profile. The calculated line-of-sight integrated tt component, $v_{tt,calc}$, scales as the square of $n_e(0)$,

$$V_{tt,calc} = \int_L \frac{1}{2} n_e^2(r) < \sigma v > (r) dL \propto n_e^2(r)$$ (5)

whereas the tt component from the neutron spectrum analysis, $v_{tt,spectrum}$, (which is line-of-sight integrated by definition) should scale as the square of $n_D(0)$,

$$V_{tt,Spectrum} = \int_L \frac{1}{2} n_D^2(r) < \sigma v > (r) dL \propto n_D^2(r)$$ (6)

The line-of-sight integrated total neutron emissivity, $v_{tot,calc}$, calculated by ORION from the neutron emission profile data (from the neutron profile camera) is

10

then assumed to be equal to the line-of-sight integrated total neutron emissivity, $v_{tot,Spectrum}$, as measured by the neutron spectrometer.

$$v_{tot,calc} = v_{tot,Spectrum} \qquad (7)$$

Combining equations (2) to(7) yields equation (8) for the value of $n_D(0)$, which is consistent with the tt component from the neutron spectrum analysis.

$$n_D(0) = n_e(0) \cdot \sqrt{f_{tt,Spectrum} / f_{tt,calc}} \qquad (8)$$

This is valid under the implicit assumption that n_D/n_e is constant throughout the plasma, i.e. the impurity mixture is constant, and the measured T_i is correct. In fig 6a, values of n_D/n_e deduced from the neutron spectrum are compared with values deduced from the optical methods (CXRS and the two visible bremsstrahlung channels). Only cases where values from more than one of the optical methods were available and in agreement within 10% have been included; their mean value has been used.

There is a considerable scatter in the data points. The statistical error in n_D/n_e from the neutron spectrum analysis is typically ±30%, which is indicated by the two outermost lines in fig 6a-b. Generally, the optical methods are most reliable when n_D/n_e is close to unity and deteriorate with decreasing values, hence, the lack of data points with small values of n_D/n_e. For n_D/n_e around 0.6, the systematic errors from the CXRS and visible Bremsstrahlung diagnostics are of the same order as the statistical errors from the neutron spectrum analysis.

By recognizing some of the intrinsic weaknesses in the neutron spectrum analysis the scatter can be reduced by imposing conditions in the same way as in section 3.1. The effect can be seen in fig 6a, where data points for which the tt fraction is larger than 0.2 are encircled.

Another useful restriction is to demand consistency between the bt fraction from the neutron spectrum analysis and that calculated with the NBI simulation code, "PENCIL" [20]. The calculated bt fraction depends mainly on the NBI power, T_e, n_e, and n_D. Using consistent values of $n_D(0)$ from eq(8) for the calculation and requiring agreement better than 30% between measured and calculated bt components leads to the data set shown in fig 6b; the scatter is visibly reduced as compared to the full data set from fig 6a.

11

4 Conclusions

Measured neutron yields and energy spectra combined with independent diagnostic data for the deuterium density, n_D, have been used to deduce the central deuterium ion temperature, T_i, for NBI heated JET discharges. Similarly, central deuterium density values have been obtained from neutron measurements combined with T_i values from independent diagnostics. Reasonable accuracy is obtained if the number of parameters deduced from the neutron spectrum analysis is kept low ($\leq$ 2) and the analysis is restricted to discharges with a relatively large tt fraction (>30% for T_i deduction and >20% for n_D deduction). Also, the analysis has to be restricted to conditions under which the spectral shape of the tt component differs sufficiently from that of the bt and bb components (T_i<12keV for 80 keV NBI). With these restrictions, results from the neutron spectrum and yield analysis agree within 30% with the T_i and n_D values obtained by independent diagnostics, which is consistent with typical experimental uncertainties of the methods. Agreement is found under conditions which lie inside the operating range of the more conventional (as opposed to neutron) diagnostics. There is no reason for the neutron spectrometer analysis to fail outside this range provided the restrictions on the tt fraction, T_i and fitting parameters are observed. The method demonstrated in this paper has potential applications in obtaining plasma parameters under conditions which lie outside the operating range of the more conventional diagnostics; it is the only reliable method available for deducing deuterium densities for plasmas with low values of n_D/n_e.

5 Acknowledgements

6 References

[1]   H W Hendel, "Neutron Yields and Spectra for Fusion Plasmas", in
       Diagnostics   for Fusion Reactor Conditions, (Varenna 1982),
       EUR 8351-I-EN, CEC, Brussels (1982)

[2]   O N Jarvis, "Neutron Detection Techniques for Plasma Diagnostics", in
       Diagnostics for Fusion Reactor Conditions, (Varenna 1982),
       EUR 8351-I-EN, CEC, Brussels (1982)

[3]   J D Strachan, "The Application of Fusion Reaction Product Diagnostics in
       Toroidal Devices", in Diagnostics for Fusion Reactor Conditions, (Varenna
       1982), EUR 8351-I-EN, CEC, Brussels (1982)

[4]   E W Lees et al., "Neutron Detection Techniques for Plasma Diagnostics at the
       Joint European Torus (JET)", Radiation Effects 95 (1986) p 253

[5]   F B Marcus et al., Europhysics Conference Abstracts, Vol 14B, part I,
       pp 331-334 (1990)

[6]   P v Belle and G Sadler, Basic and Advanced Diagnostic Techniques for Fusion
       Plasmas (Proc Course and Workshop, Varenna 1986) Vol III, EUR 10797 EN,
       CEC (1987) 767, and references therein.

[7]   G Sadler et al., Europhysics Conference Abstracts, Vol 14B, part I, p 1 (1990)
       and J M Adams et al, "Studies of D-D fusion reactivity in high
       temperature JET plasmas", Nuclear Fusion, vol 31, no 5 (1991), p 891

[8]   O N Jarvis et al, Nuclear Fusion, 28, No 11 (1988), p 1981

[9]   T Elevant et al., "The JET neutron time-of-flight spectrometer",
       Nuclear Instruments and Methods in Physics Research A306 (1991)

[10]   M J Loughlin et al, Nuclear Instruments and Methods in Physics Research,
       A281 (1989) 184-191, North Holland, Amsterdam

[11]   W H Press, B P Flannery, S A Teukolsky and W T Vetterling, Numerical
       Recipes, Cambridge University Press 1986, p 534

[12]   H Weisen, M von Hellermann, A Boileau. L Horton, W Mandl, H P Summers,
       Nuclear Fusion, 29, p 2187 (1989)

[13]   R Bartiromo et al, "The JET High Resolution Bent Crystal Spectrometer",
       Rev Sci Inst, 60, p 237 (1989)

[14]   J G Cordey, W G F Core and J Sheffield, Nuclear Fusion 17 (1975), p 755.

[15]   D Veron, in Diagnostics for Fusion Reactor Conditions, (Proc Workshop
       Varenna 1982), EUR 8351-II-EN, CEC, Brussels (1982) 283.

[16]   P D Morgan, in Controlled Fusion and Plasma Heating, (Proc 15th Eur Conf
       Dubrovnik, 1988), Vol 12B, Part I, European Physical Society (1988) 139.

[17]   (a) H Salzmann, K Hirsch, P Nielsen, et al, Nucl Fusion <u>27</u> (1987) 1925.

        (b) H Salzmann, J Bundgaard, A Gadd, et al, Rev Sci Instrum <u>59</u> (1988) 1451.

[18]   D V Bartlett, D J Campbell, A E Costley, et al, Electron Cyclotron Emission and Electron Cyclotron Resonance Heating (Proc 6th Int Workshop, Oxford, 1987), UKAEA, Culham Laboratory (1987) 137.

[19]   S Conroy, PhD-thesis, Imperial College, London, UK

[20]   R J Goldston et al, J Comput Phys, <u>43</u>, p 61 (1981)

[21]   P M Stubberfield and M L Watkins, JET Internal Report, DPA(06)/87 (1987)

Figure captions

Fig 1

Showing the neutron time-of-flight spectrometer in the JET roof laboratory. The time-of-flight between a neutron interaction in the first detector, which is denoted D_0, and a subsequent interaction by the same neutron in the second detector, denoted D_1, is measured. There are 12 D_1 detectors for increased efficiency. All detectors consist of fast plastic scintillators optically coupled to photomultiplier tubes and the neutrons interact through elastic scattering on protons in the plastic.

Fig 2

a) Measured neutron spectrum from a Maxwellian plasma (#15383). The plasma is ICRF heated with the RF tuned to ^3He minority ions. Carbon is the main first wall material and plasma impurity. The Gaussian shaped spectrum is typical for Maxwellian plasmas.

b) Measured neutron spectrum from a non-Maxwellian plasma, which is heated by 80 keV deuterium neutral beam injection (#20180). The spectrum is considerably broadened due to the high energy of the reacting beam-ions.

c) Measured neutron spectrum from a plasma which is non-Maxwellian due to deuterium NBI combined with ICRF heating tuned to protons (= 2nd harmonic for deuterons) (#20725). There is a clear indication of a high energy tail due to an ICRF accelerated component in the plasma, reacting with thermal deuterons and/or Beryllium impurity ions.

Fig 3

a) bb and bt spectra calculated with the FPS code and the Gaussian tt component, used for the unfolding of the measured neutron spectrum from fig 2b. The temperature of the target plasma used in the calculations is 5 keV.

b) The spectra from fig 3a folded with the instrumental response of the time-of-flight spectrometer.

c) The resulting fit of the folded spectra from fig 3b to the measured spectrum of fig 2b.

d) The underlying (=unfolded) neutron spectrum obtained by adding up the non-folded bb, bt and tt spectra in the proportions given by the fit in fig 3c.

Fig 4

The tt fraction as a function of the central T_i. The crosses show values calculated using the independently measured n_D values reflect the dependence of the fusion reactivity on T_i. The circles show the tt fraction as a function of T_i $_{guess}$ from the neutron spectrum analysis. Consistency between the measured n_D and the neutron spectrum is obtained at the intersection of the two curves.

Fig 5

Comparison of consistent T_i values from neutron diagnostics with T_i values from optical measurements. Applying the condition; tt fraction > 0.3 and T_i < 12 keV and $n_D(0)/n_e(0)$ > 0.4 (encircled data points) reduces the scatter significantly.

Fig 6

a) Plot of n_D/n_e obtained from CXRS and/or visible bremsstrahlung as a function of n_D/n_e deduced from neutron spectrum analysis, T_i and neutron emission. Only cases where values from more than one of the optical methods were available and in agreement within 10% have been included and their mean value has been used. The full lines correspond to a typical statistical error of ±30% in n_D/n_e from the neutron spectrum analysis. Data points for which the tt fraction is larger than 0.2 are encircled.

b) The same plot as in fig 6.a, but the data points now refer to cases for which the bt fraction from the spectrum analysis agrees with PENCIL code calculations within 30%. For these calculations consistent n_D values were used as opposed to their usual derivation from n_e and Z_{eff}.
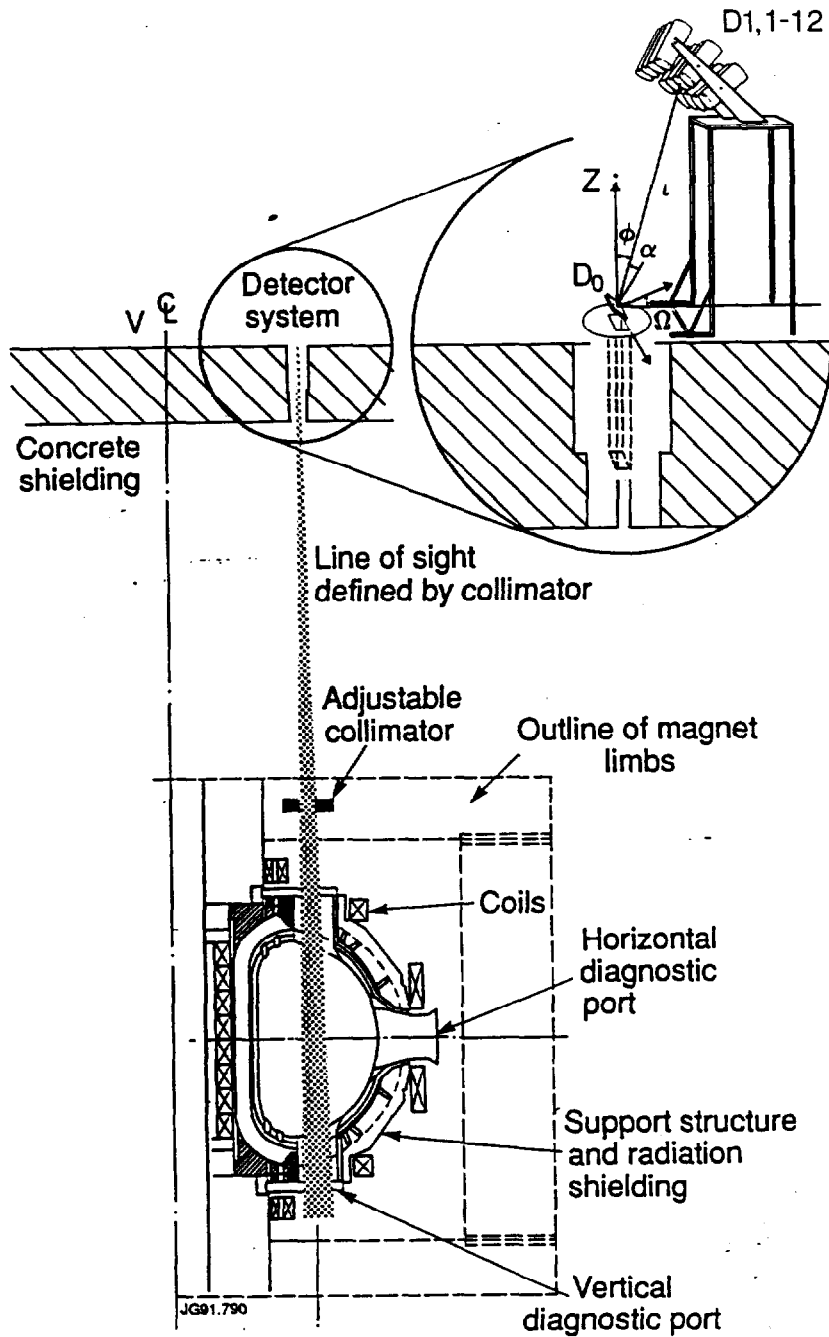
Fig 1

Showing the neutron time-of-flight spectrometer in the JET roof laboratory. The time-of-flight between a neutron interaction in the first detector, which is denoted D_0, and a subsequent interaction by the same neutron in the second detector, denoted D_1, is measured. There are 12 D_1 detectors for increased efficiency. All detectors consist of fast plastic scintillators optically coupled to photomultiplier tubes and the neutrons interact through elastic scattering on protons in the plastic.

Fig 2

Fig 2

a) Measured neutron spectrum from a Maxwellian plasma (#15383).   The plasma is ICRF heated with the RF tuned to 3He minority ions.   Carbon is the main first wall material and plasma impurity. The Gaussian shaped spectrum is typical for Maxwellian plasmas.

b) Measured neutron spectrum from a non-Maxwellian plasma, which is heated by 80 keVdeuterium neutral beam injection (#20180).   The spectrum is considerably broadened due to the high energy of the reacting beam-ions.

c) Measured neutron spectrum from a plasma which is non-Maxwellian due to deuterium NBI combined with ICRF heating tuned to protons (= 2nd harmonic for deuterons) (#20725).   There is a clear indication of a high energy tail due to an ICRF accelerated component in the plasma, reacting with thermal deuterons and/or Beryllium impurity ions.
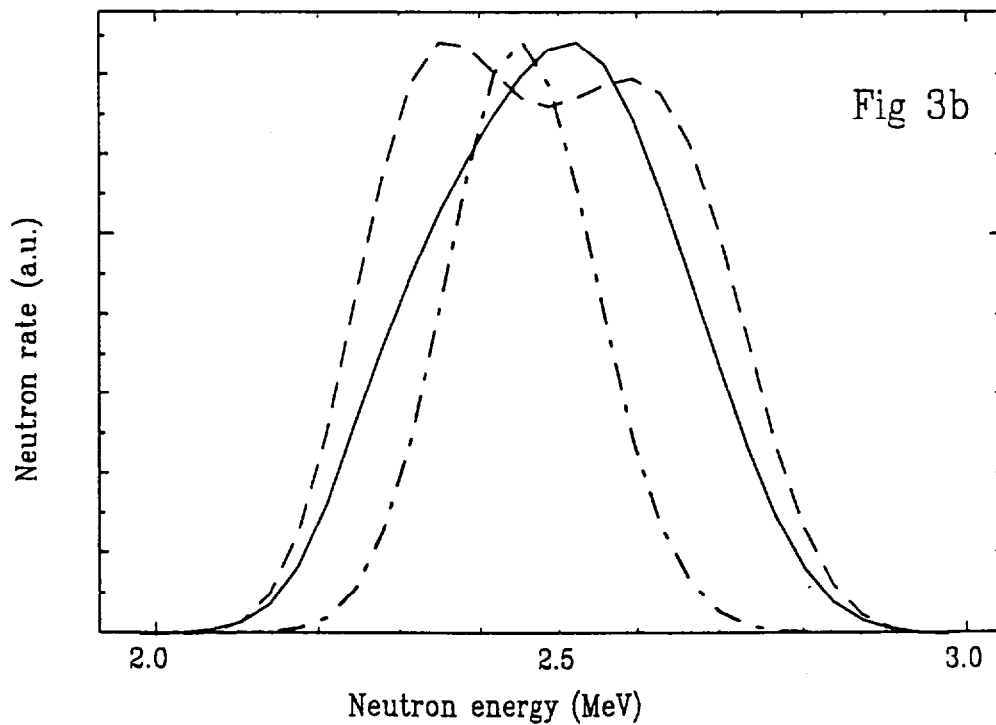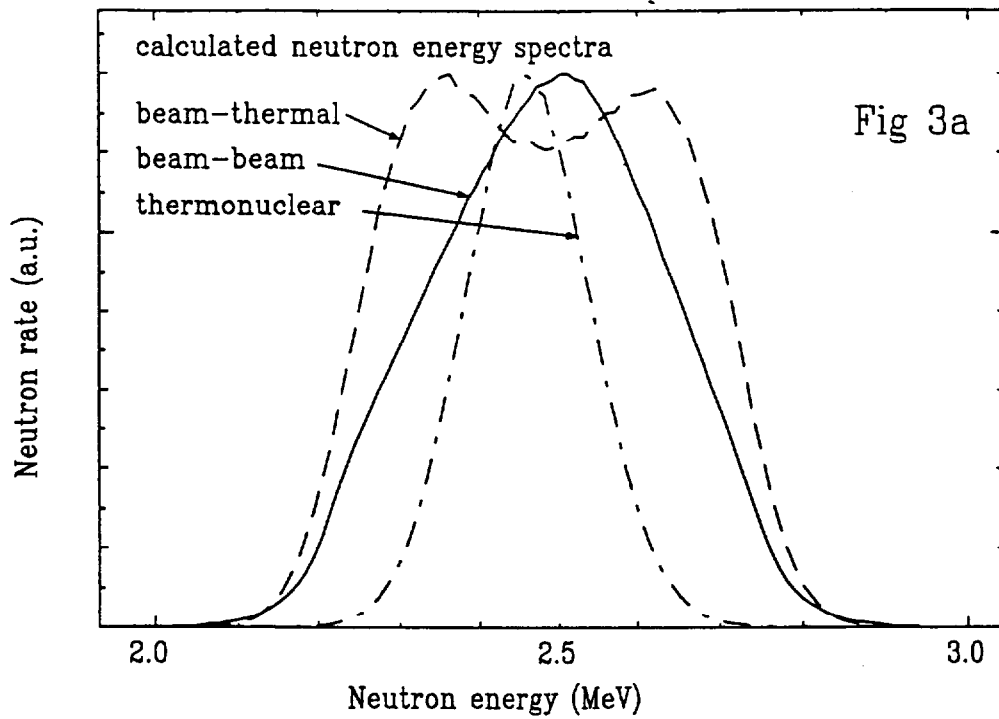
Fig 3

a) bb and bt spectra calculated with the FPS code and the Gaussian tt component, used for the unfolding of the measured neutron spectrum from fig 2b. The temperature of the target plasma used in the calculations is 5 keV.

b) The spectra from fig 3a folded with the instrumental response of the time-of-flight spectrometer.
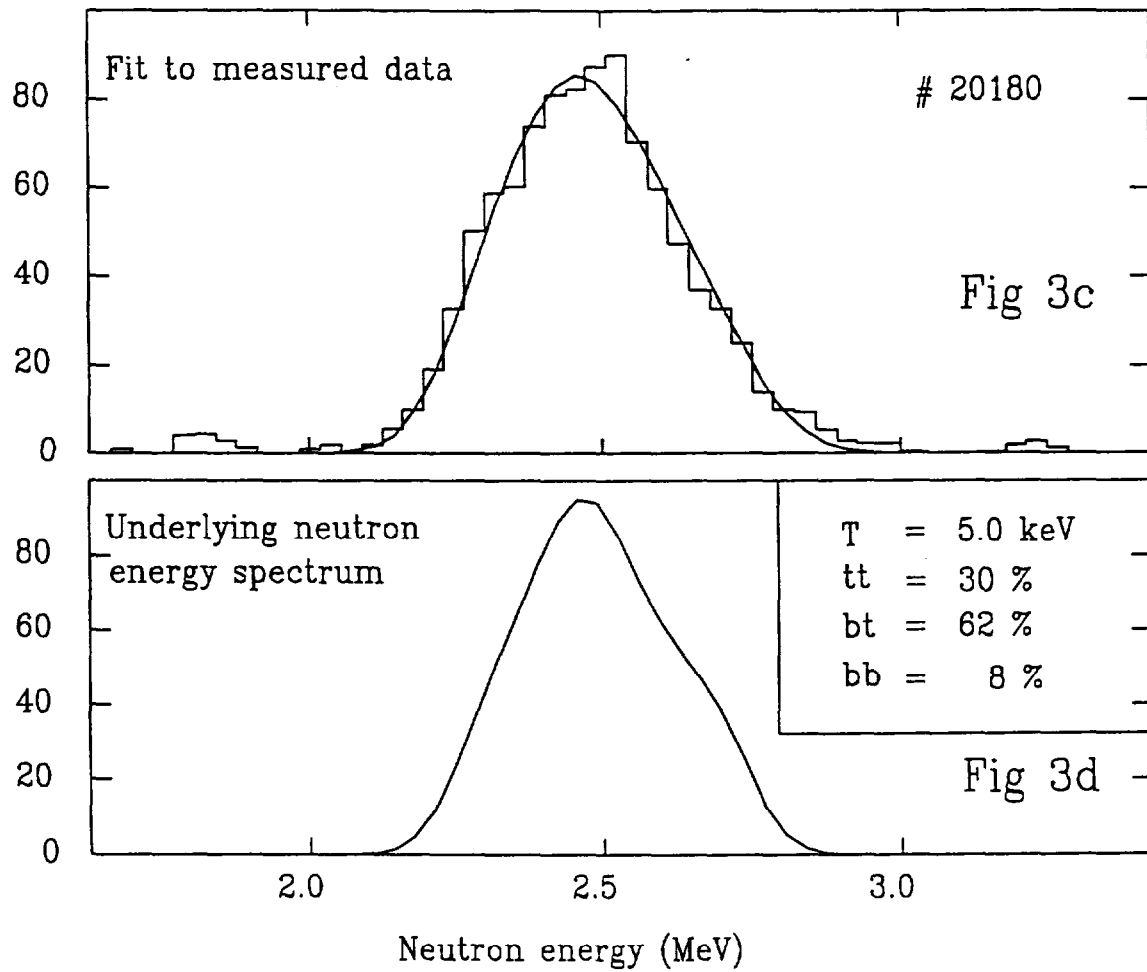
Fig 3
c) The resulting fit of the folded spectra from fig 3b to the measured spectrum of
fig 2b.
d) The underlying (=unfolded) neutron spectrum obtained by adding up the non folded
bb, bt and tt spectra in the proportions, given by the fit in fig 3c.
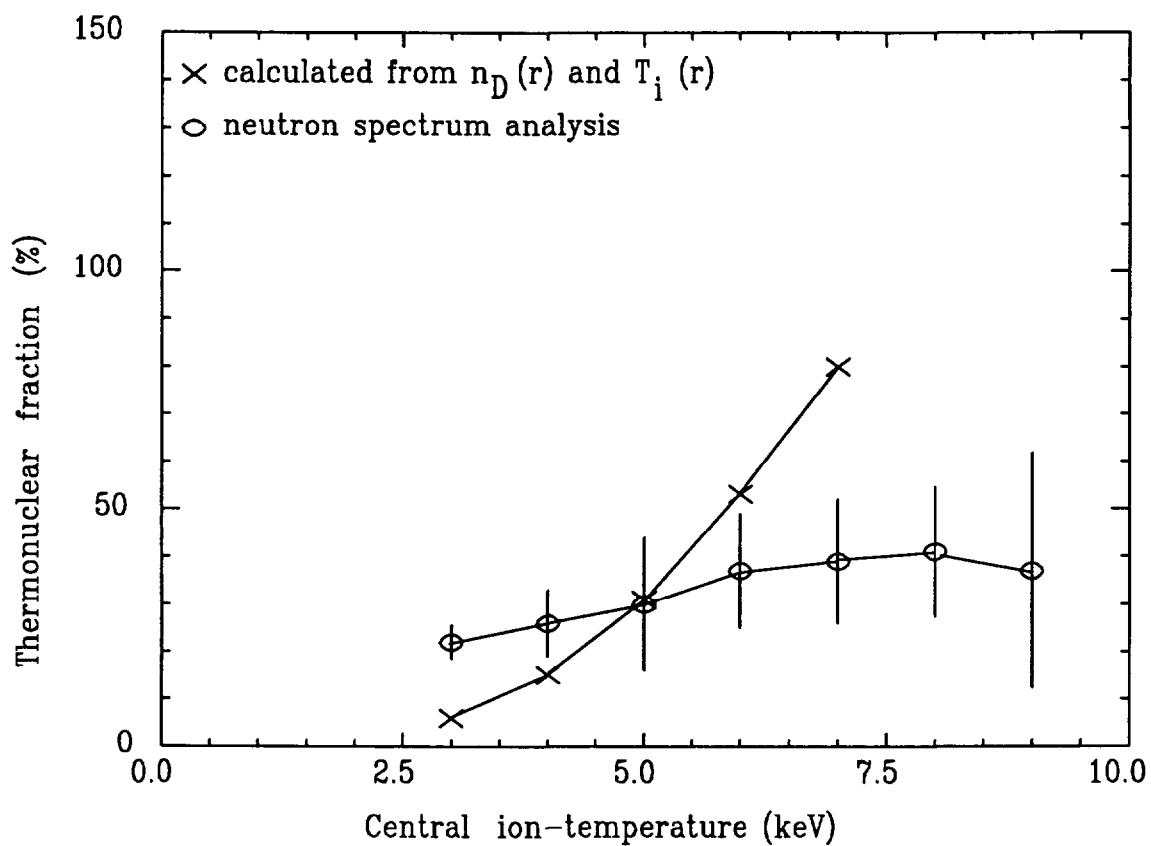
Fig 4

Fig 4

The tt fraction as a function of the central Ti. The crosses show values calculated using the independently measured n_D values and reflect the dependence of the fusion reactivity on Ti. The circles show the tt fraction as a function of Ti guess from the neutron spectrum analysis. Consistency between the measured $\dot{n}D$ and the neutron spectrum is obtained at the intersection of the two curves.
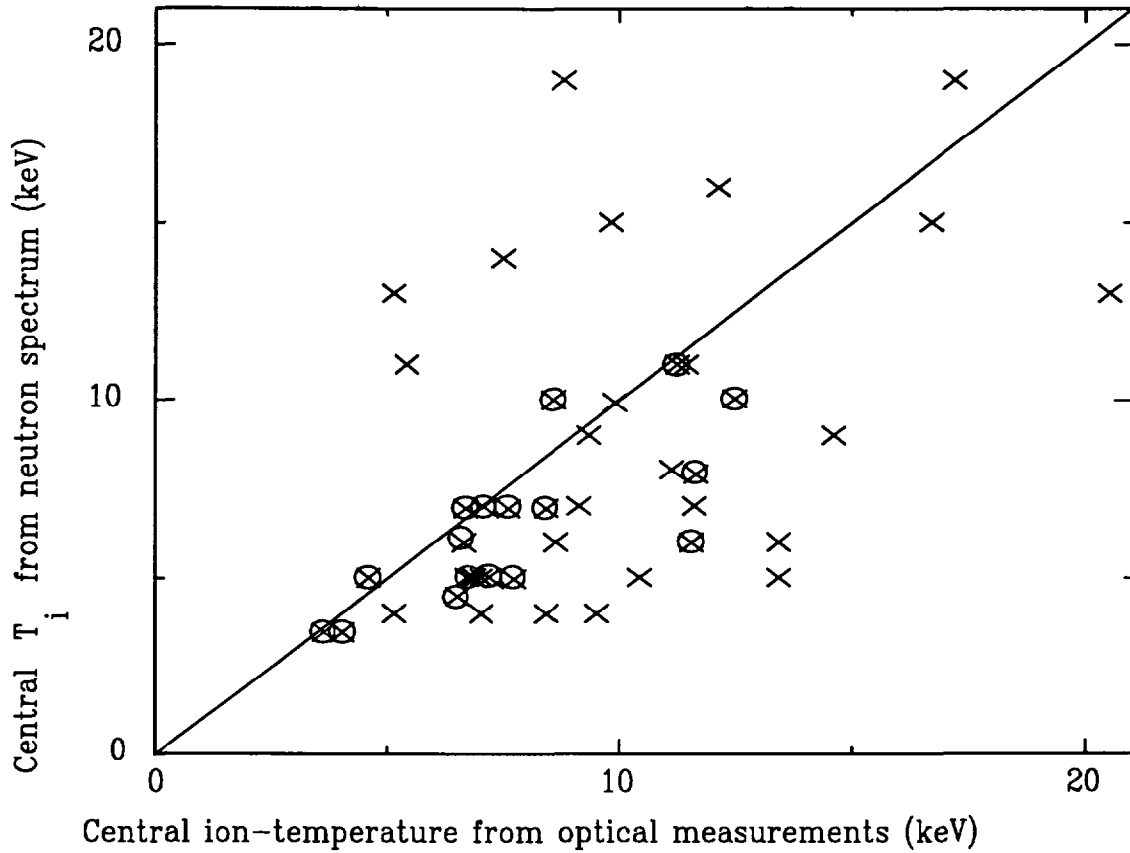
Fig 5

Fig 5
Comparison of consistent Ti values from neutron diagnostics with Ti values from optical measurements. Applying the condition; tt fraction > 0.3 and Ti < 12 keV and nD(0)/ne(0) > 0.4 (encircled data points) reduces the scatter.
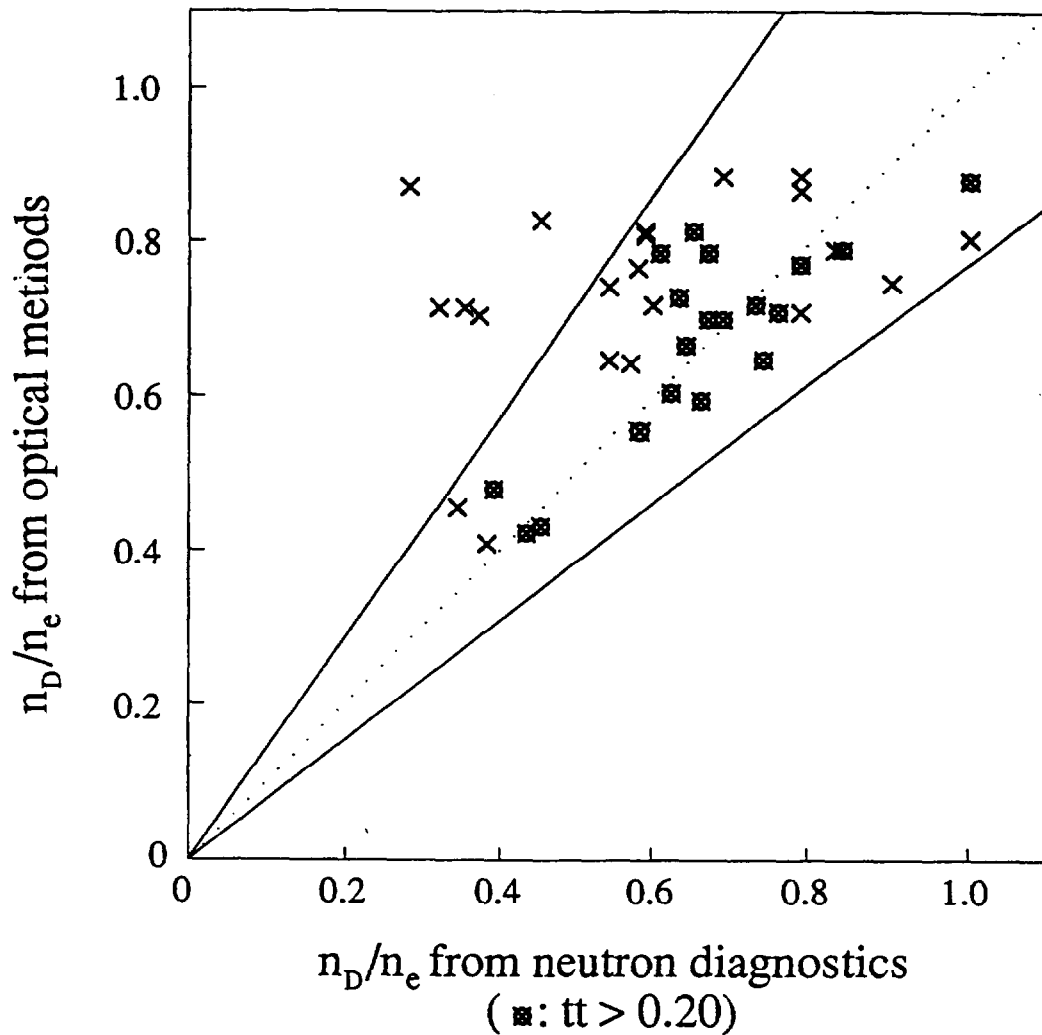
Fig 6a

Fig 6 a

Plot of n_D/n_e obtained from CXRS and/or visible bremsstrahlung as a function of n_D/n_e deduced from neutron spectrum analysis, T_i and neutron emission. Only cases where values from more than one of the optical methods were available and in agreement within 10% have been included and their mean value has been used. The full lines correspond to a typical statistical error of ±30% in n_D/n_e from the neutron spectrum analysis. Data points for which the tt fraction is larger than 0.2 are encircled.
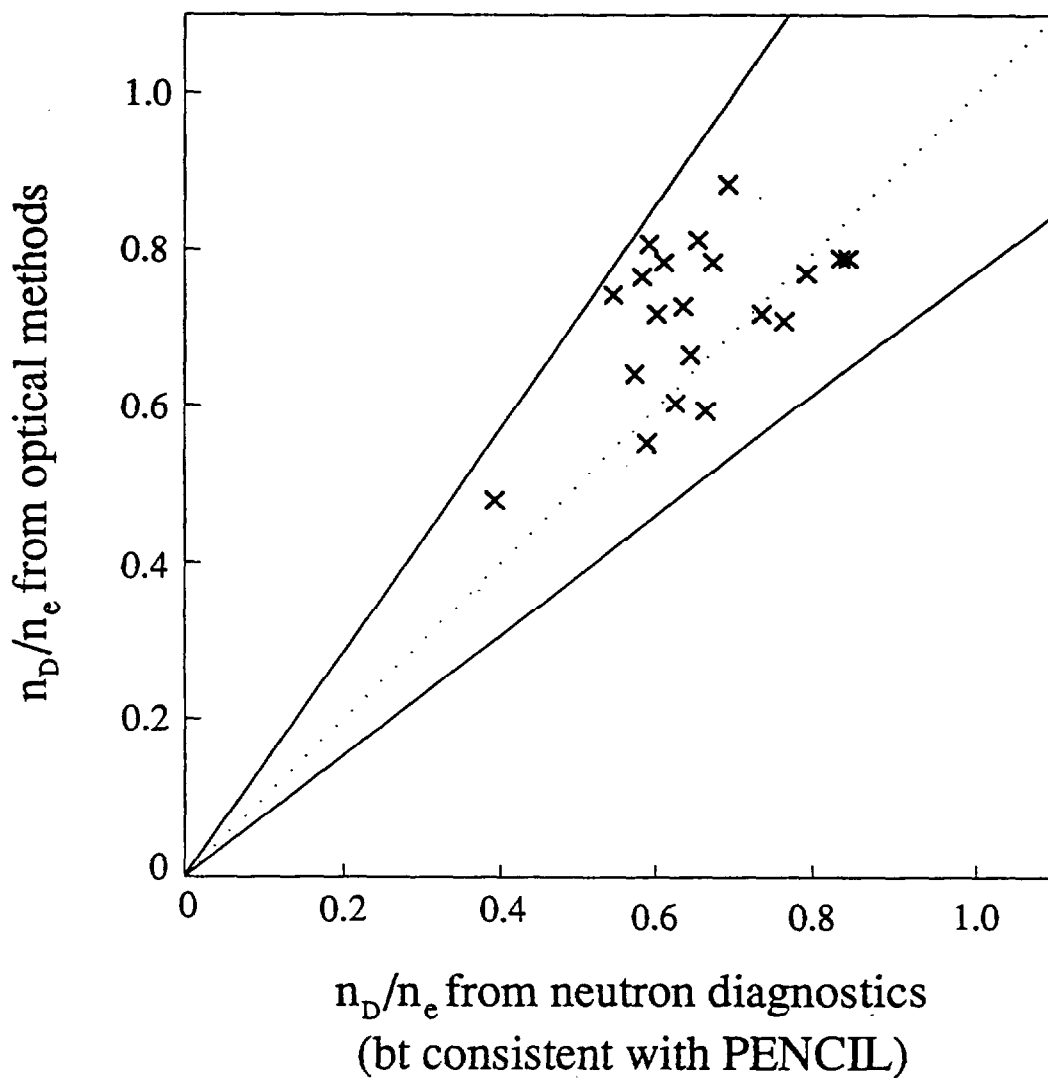
Fig 6b

Fig 6 b

The same plot as in fig 6.a, but the data points now refer to cases for which the bt fraction from the spectrum analysis agrees with PENCIL code calculations within 30%. For these calculations consistent n_D values were used as opposed to their usual derivation from n_e and Z_{eff}.

ANNEX

P.-H. REBUT, A. GIBSON, M. HUGUET, J.M. ADAMS[1], B. ALPER, H. ALTMANN, A. ANDERSEN[2], P. ANDREW[3],

M. ANGELONE[4], S. ALI-ARSHAD, P. BAIGGER, W. BAILEY, B. BALET, P. BARABASCHI, P. BARKER, R. BARNSLEY[5],

M. BARONIAN, D.V. BARTLETT, L. BAYLOR[6], A.C. BELL, G. BENALI, P. BERTOLDI, E. BERTOLINI, V. BHATNAGAR,

A.J. BICKLEY, D. BINDER, H. BINDSLEV[2], T. BONICELLI, S.J. BOOTH, G. BOSIA, M. BOTMAN, D. BOUCHER,

P. BOUCQUEY, P. BREGER, H. BRELEN, H. BRINKSCHULTE, D. BROOKS, A. BROWN, T. BROWN, M. BRUSATI,

S. BRYAN, J. BRZOZOWSKI[7], R. BUCHSE[22], T. BUDD, M. BURES, T. BUSINARO, P. BUTCHER, H. BUTTGEREIT,

C. CALDWELL-NICHOLS, D.J. CAMPBELL, P. CARD, G. CELENTANO, C.D. CHALLIS, A.V. CHANKIN[8], A. CHERUBINI,

D. CHIRON, J. CHRISTIANSEN, P. CHUILON, R. CLAESEN, S. CLEMENT, E. CLIPSHAM, J.P. COAD, I.H. COFFEY[9],

A. COLTON, M. COMISKEY[10], S. CONROY, M. COOKE, D. COOPER, S. COOPER, J.G. CORDEY, W. CORE, G. CORRIGAN,

S. CORTI, A.E. COSTLEY, G. COTTRELL, M. COX[11], P. CRIPWELL[12], O. Da COSTA, J. DAVIES, N. DAVIES, H. de BLANK,

H. de ESCH, L. de KOCK, E. DEKSNIS, F. DELVART, G.B. DENNE-HINNOV, G. DESCHAMPS, W.J. DICKSON[13], K.J. DIETZ,

S.L. DMITRENKO, M. DMITRIEVA[14], J. DOBBING, A. DOGLIO, N. DOLGETTA, S.E. DORLING. P.G. DOYLE, D.F. DÜCHS,

H. DUQUENOY, A. EDWARDS, J. EHRENBERG, A. EKEDAHL, T. ELEVANT[7], S.K. ERENTS[11], L.G. ERIKSSON,

H. FAJEMIROKUN[12], H. FALTER, J. FREILING[15], F. FREVILLE, C. FROGER, P. FROISSARD, K. FULLARD, M. GADEBERG,

A. GALETSAS, T. GALLAGHER, D. GAMBIER, M. GARRIBBA, P. GAZE, R. GIANNELLA, R.D. GILL, A GIRARD,

A. GONDHALEKAR, D. GOODALL[11], C. GORMEZANO, N.A. GOTTARDI, C. GOWERS, B.J. GREEN, B. GRIEVSON, R. HAANGE,

A. HAIGH, C.J. HANCOCK, P.J. HARBOUR, T. HARTRAMPF, N.C. HAWKES[11], P. HAYNES[11], J.L. HEMMERICH, T. HENDER[11],

J. HOEKZEMA, D. HOLLAND, M. HONE, L. HORTON, J. HOW, M. HUART, I. HUGHES, T.P. HUGHES[10], M. HUGON, Y. HUO[16],

K. IDA[17], B. INGRAM, M. IRVING, J. JACQUINOT, H. JAECKEL, J.F. JAEGER, G. JANESCHITZ, Z. JANKOVICZ[18], O.N. JARVIS,

F. JENSEN, E.M. JONES, H.D. JONES, L.P.D.F. JONES, S. JONES[19], T.T.C. JONES, J.-F. JUNGER, F. JUNIQUE, A. KAYE,

B.E. KEEN, M. KEILHACKER, G.J. KELLY, W. KERNER, A. KHUDOLEEV[21], R. KONIG, A. KONSTANTELLOS, M. KOVANEN[20],

G. KRAMER[15], P. KUPSCHUS, R. LÄSSER, J.R. LAST, B. LAUNDY, L. LAURO-TARONI, M. LAVEYRY, K. LAWSON[11],

M. LENNHOLM, J. LINGERTAT[22], R.N. LITUNOVSKI, A. LOARTE, R. LOBEL, P. LOMAS, M. LOUGHLIN, C. LOWRY, J. LUPO,

A.C. MAAS[15], J. MACHUZAK[19], B. MACKLIN, G. MADDISON[11], C.F. MAGGI[23], G. MAGYAR, W. MANDL[22], V. MARCHESE,

G. MARCON, F. MARCUS, J. MART, D. MARTIN, E. MARTIN, R. MARTIN-SOLIS[24], P. MASSMANN, G. MATTHEWS,

H. McBRYAN, G. McCRACKEN[11], J. McKIVITT, P. MERIGUET, P. MIELE, A. MILLER, J. MILLS, S.F. MILLS, P. MILLWARD,

P. MILVERTON, E. MINARDI[4], R. MOHANTI[25], P.L. MONDINO, D. MONTGOMERY[26], A. MONTVAI[27], P. MORGAN,

H. MORSI, D. MUIR, G. MURPHY, R. MYRNÄS[28], F. NAVE[29], G. NEWBERT, M. NEWMAN, P. NIELSEN, P. NOLL,

W. OBERT, D. O'BRIEN, J. ORCHARD, J. O'ROURKE, R. OSTROM, M. OTTAVIANI, M. PAIN, F. PAOLETTI,

S. PAPASTERGIOU, W. PARSONS, D. PASINI, D. PATEL, A. PEACOCK, N. PEACOCK[11], R.J.M. PEARCE, D. PEARSON[12],

J.F. PENG[16], R. PEPE DE SILVA, G. PERINIC, C. PERRY, M. PETROV[21], M.A. PICK, J. PLANCOULAINE, J.-P POFFÉ,

R. PÖHLCHEN, F. PORCELLI, L. PORTE[13], R. PRENTICE, S. PUPPIN, S. PUTVINSKII[8], G. RADFORD[30], T. RAIMONDI,

M.C. RAMOS DE ANDRADE, R. REICHLE, J. REID, S. RICHARDS, E. RIGHI, F. RIMINI, D. ROBINSON[11], A. ROLFE,

R.T. ROSS, L. ROSSI, R. RUSS, P. RUTTER, H.C. SACK, G. SADLER, G. SAIBENE, J.L. SALANAVE, G. SANAZZARO,

A. SANTAGIUSTINA, R. SARTORI, C. SBORCHIA, P. SCHILD, M. SCHMID, G. SCHMIDT[31], B. SCHUNKE, S.M. SCOTT,

L. SERIO, A SIBLEY, R. SIMONINI, A.C.C. SIPS, P. SMEULDERS, R. SMITH, R. STAGG, M. STAMP, P. STANGEBY[3],

R. STANKIEWICZ[32], D.F. START, C.A. STEED, D. STORK, P.E. STOTT, P. STUBBERFIELD, D. SUMMERS, H. SUMMERS[13],

L. SVENSSON, J.A. TAGLE[33], M. TALBOT, A. TANGA, A. TARONI, C. TERELLA, A TERRINGTON, A TESINI, P.R. THOMAS,

E. THOMPSON, K. THOMSEN, F. TIBONE, A. TISCORNIA, P. TREVALION, B. TUBBING, P. VAN BELLE, H. VAN DER BEKEN,

G. VLASES, M. VON HELLERMANN, T. WADE, C. WALKER, R. WALTON[31], D. WARD, M.L. WATKINS, N. WATKINS,

M.J. WATSON, S. WEBER[34], J. WESSON, T.J. WIJNANDS, J. WILKS, D. WILSON, T. WINKEL, R. WOLF, D. WONG,

C. WOODWARD, Y. WU[35], M. WYKES, D. YOUNG, I.D. YOUNG, L. ZANNELLI, A. ZOLFAGHARI[19], W. ZWINGMANN

18

[1] Harwell Laboratory, UKAEA, Harwell, Didcot, Oxfordshire, UK.
[2] Risø National Laboratory, Roskilde, Denmark.
[3] Institute for Aerospace Studies, University of Toronto, Downsview, Ontario, Canada.
[4] ENEA Frascati Energy Research Centre, Frascati, Rome, Italy.
[5] University of Leicester, Leicester, UK.
[6] Oak Ridge National Laboratory, Oak Ridge, TN, USA.
[7] Royal Institute of Technology, Stockholm, Sweden.
[8] I.V. Kurchatov Institute of Atomic Energy, Moscow, Russian Federation.
[9] Queens University, Belfast, UK.
[10] University of Essex, Colchester, UK.
[11] Culham Laboratory, UKAEA, Abingdon, Oxfordshire, UK.
[12] Imperial College of Science, Technology and Medicine, University of London, London, UK.
[13] University of Strathclyde, Glasgow, UK.
[14] Keldysh Institute of Applied Mathematics, Moscow, Russian Federation.
[15] FOM-Institute for Plasma Physics "Rijnhuizen", Nieuwegein, Netherlands.
[16] Institute of Plasma Physics, Academia Sinica, Hefei, Anhui Province, China.
[17] National Institute for Fusion Science, Nagoya, Japan.
[18] Soltan Institute for Nuclear Studies, Otwock/Świerk, Poland.
[19] Plasma Fusion Center, Massachusetts Institute of Technology, Boston, MA, USA.
[20] Nuclear Engineering Laboratory, Lappeenranta University, Finland.
[21] A.F. Ioffe Physico-Technical Institute, St. Petersburg, Russian Federation.
[22] Max-Planck-Institut für Plasmaphysik, Garching, Germany.
[23] Department of Physics, University of Milan, Milan, Italy.
[24] Universidad Complutense de Madrid, Madrid, Spain.
[25] North Carolina State University, Raleigh, NC, USA.
[26] Dartmouth College, Hanover, NH, USA.
[27] Central Research Institute for Physics, Budapest, Hungary.
[28] University of Lund, Lund, Sweden.
[29] Laboratorio Nacional de Engenharia e Tecnologia Industrial, Sacavem, Portugal.
[30] Institute of Mathematics, University of Oxford, Oxford, UK.
[31] Princeton Plasma Physics Laboratory, Princeton University, Princeton, NJ, USA.
[32] RCC Cyfronet, Otwock/Świerk, Poland,
[33] Centro de Investigaciones Energéticas, Medioambientales y Tecnológicas, Madrid, Spain.
[34] Freie Universität, Berlin, Germany.
[35] Insitute for Mechanics, Academia Sinica, Beijing, China.